Evaluation of Pore Structure Parameters of MCM-41 Catalyst Supports and Catalysts by Means of Nitrogen and Argon Adsorption

P. I. Ravikovitch,[†] D. Wei,[†] W. T. Chueh,[†] G. L. Haller,*[,†] and A. V. Neimark[†,‡]

Department of Chemical Engineering, Yale University, New Haven, Connecticut 06520-8286, and TRI/Princeton, Princeton, New Jersey 08542

Received: August 16, 1996; In Final Form: December 29, 1996[⊗]

A new method has been used to obtain pore size characteristics of MCM-41 catalyst supports and vanadium-substituted MCM-41 catalysts. The approach is based on the nonlocal density functional theory (NLDFT) model for nitrogen and argon adsorption in MCM-41, proposed recently. Samples with pore sizes varying from ca. 25 to 37 Å were prepared by hydrothermal synthesis. Two synthesis procedures employing different sources of V were used to prepare V/MCM-41 catalysts. The samples were characterized by X-ray diffraction (XRD). N_2 and Ar adsorption isotherms at 77 K were measured starting from the relative pressure $P/P_0 = 1 \times 10^{-5}$. Analysis of adsorption isotherms was carried out in two stages. The first stage implies comparison of a given isotherm with a reference isotherm measured on a well-characterized sample of MCM-41 with uniform pores. From such a comparison, micropore volume, specific surface area of mesopores, and the point of the beginning of the capillary condensation are determined. In the second stage, pore size distributions are calculated from the NLDFT. Pore size distributions obtained from N_2 and Ar isotherms at 77 K were in perfect agreement. These results were compared with the traditional Barrett−Joyner−Halenda (BJH) method, and with the XRD data. It is shown that the BJH method underestimates an average pore size in MCM-41 materials by ca. 10 Å. Adsorption studies of V/MCM-41 catalysts revealed that the synthesis procedure with the direct addition of V_2O_5 yields samples with a more uniform pore structure than the procedure with the use of $VOSO_4 \cdot 3H_2O$ solution.

Introduction

Porous materials have found great utility as catalysts for industrial applications. Their large surface areas enhance the catalytic and sorptive activity. Amorphous mesoporous materials represent an important class of porous inorganic solids which have no long-range order and usually have a wide distribution of pore sizes. In contrast, microporous molecular sieves have a crystalline structure with a very narrow pore size distribution. It is generally presumed that a mesoporous material with uniform pores would have wide utility in catalysis. Therefore, considerable synthetic effort has been devoted to developing frameworks with pore diameters within the mesoporous range.

Recently, a new family of mesoporous molecular sieves designated as M41S was discovered by Mobil scientists.[1−3] The MCM-41 materials possess a regular array of hexagonal, uniform, unidimensional mesopores, which can be systematically varied in size from around 16 to 100 Å.[2] These materials bridge the gap between uniform microporous and amorphous mesoporous materials. Such unique characteristics, together with the high surface area (up to 1000 m^2g^{-1}) and distinct adsorption properties,[4] open up new potential applications.

Like in zeolites, the framework of MCM-41 is based on an extensive three-dimensional network of oxygen ions that occupied tetrahedral cation sites, and in addition to the Si^{4+}, other cations can also occupy these sites. The unique properties of zeolites with transition metals incorporated have opened many new possibilities in catalysis, especially in selective oxidation of organic compounds. There is no doubt that there exists a strong incentive to use MCM-41, which can deal with bigger molecules and provide better mass transport than zeolites.[5−7] Preparation of the vanadium-substituted MCM-41 materials has been reported.[5] It was found that they were very active catalysts in the selective oxidation of hydrocarbons by H_2O_2 in liquid phase reaction, especially for larger molecules.

Development of new catalysts requires reliable methods for their characterization. Several methods are commonly used to characterize the pore structure in MCM-41 materials.[8] All of them have limited utility, and only a combination of methods can give complete information. For example, X-ray diffraction (XRD) does not provide information about the portion of the sample which is not ordered and, without an independent measure of the wall thickness, does not measure directly the internal pore size. Transmission electron microscopy (TEM) gives a direct picture of pores but samples only a very small fraction of the material,[8] so that in order to obtain reliable information, a large number of measurements has to be carried out, unless there is independent evidence of homogeneity.

In contrast, physical adsorption isotherms have the advantage of producing a macroscopic average measurement, from which such characteristics as specific surface area, micro- and mesopore volume, and pore size distribution (PSD) are obtained.[9] However, application of classical thermodynamic methods for calculating PSD[9] in materials with the pore size of the order of nanometers is questionable and may give incorrect results.[10] New methods, based on the statistical thermodynamics approaches, such as density functional theory (DFT) and Monte Carlo simulations (MC) are very promising.[10−12]

A nonlocal density functional theory (NLDFT) model of adsorption on MCM-41 has been proposed recently.[13,14] The model has been tested on the reference MCM-41 materials with presumably uniform pore structure.[15] Here, we apply this model for calculating PSDs in MCM-41-based catalyst supports, prepared using surfactants with different chain length, and in V/MCM-41 catalysts prepared using two different sources of

[†] Department of Chemical Engineering.
[‡] TRI/Princeton.
[⊗] Abstract published in *Advance ACS Abstracts,* April 1, 1997.

S1089-5647(96)02532-1 CCC: $14.00

V. Our analysis consists of two stages. In the first step, experimental N_2 and Ar adsorption isotherms are compared with isotherms on a well-characterized siliceous MCM-41, taken as a reference sample. Then, the PSDs are calculated from N_2 and Ar isotherms using the NLDFT approach. An average pore size obtained from the PSD analysis and XRD data are used to obtained the pore wall thickness. The results are compared with those obtained from the traditional BJH method.

Thus, the purpose of this paper is to characterize the pore structure in MCM-41 catalyst supports and V/MCM-41 catalysts and to demonstrate the utility of the NLDFT-based approach for calculating pore size distributions.

Experimental Section

Synthesis. *Materials.* Silica sources were HiSil-233 from Pittsburgh Plate Glass (PPG) and tetramethylammonium silicate (10 wt % silica) from SACHEM, Inc. The vanadium sources were $VOSO_4 \cdot 3H_2O$ and V_2O_5 from Aldrich Chemical Co. The quaternary ammonium surfactants $C_nH_{2n+1}(CH_3)_3NBr$ were purchased from Sigma Co. with $n = 12$, 14, and 16 and were from American Tokyo Kasei with $n = 8$ and 10. The $C_nH_{2n+1}(CH_3)_3NOH$ ($n = 8$, 10, 12, 14, and 16) solutions were prepared by ion exchanging the 29 wt % of $C_nH_{2n+1}(CH_3)_3$-NBr aqueous solution with equal molar exchange capacity of IRA-400(OH) ion exchange resin (Aldrich Chemical Co.) by batch mixing.

Siliceous MCM-41 Catalyst Supports. Two hundred grams of the $C_nH_{2n+1}(CH_3)_3NOH$ ($n = 8$, 10, 12, 14, and 16) solutions were combined with 100 g of tetramethylammonium silicate, and after mixing well, 25 g of HiSil-233 was added to each mixture with stirring. Then they were placed in an autoclave at 150 °C for 48 h. After cooling to room temperature, the resulting solid was recovered by filtering on a Büchner funnel, washing with water, and drying in air at ambient temperature.

Vanadium-Substituted MCM-41 Samples. The $C_nH_{2n+1}(CH_3)_3$-NOH ($n = 14$ and 16) solutions were combined with tetramethylammonium silicate and HiSil-233, respectively, with stirring. The $VOSO_4 \cdot 3H_2O$ was dissolved in water first and then added to the above mixtures; the V_2O_5 was added directly. The molar ratio of the components was controlled at SiO_2: $VOSO_4 \cdot (V_2O_5)$:ROH = 1:0.167 (0.334):0.5. After stirring for 30 min, they were placed in an autoclave at 120 °C for 6 days. After cooling to room temperature, the resulting solid was recovered by filtering on a Büchner funnel, washing with water, and drying in air at ambient temperature.

In both cases, the predried solid was loaded into a glass reactor which had a ceramic distributor of the inlet gas. It was heated from room temperature to 540 °C in a flow of UHP helium over a period of 20 h, followed by 1 h in UHP helium and 5 h in a flow of UHP oxygen at 540 °C.

The preparation process may cause some loss of vanadium in the products, thus all vanadium-substituted samples have been analyzed by ICP (Galbraith Laboratories, Inc.). The actual vanadium loadings have been determined to be ca. 0.40 wt %. The sample codes are explained in Table 1.

X-ray Diffraction. The Cu Kα, $\lambda = 0.154$ nm, X-rays produced by a RU-300 Rigaku rotating anode generator at 50 kV and 180 mA, were monochromated by diffraction from flat pyrolytic graphite. The collimator was a 600 nm long pipe filled with helium. The detector was a two-dimensional, position sensitive detector (Hamlin) with 256 × 144 pixels and a sensitive area of 290 × 256 mm^2. Data-collecting time was 100 s. All measurements were made at room temperature.

Adsorption Isotherms. Adsorption−desorption isotherms of N_2 and Ar at 77 K have been measured with the static volumetric instrument Autosorb-1C (Quantachrome). The samples were outgassed at 200 °C to a residual pressure lower than 1×10^{-4} Torr. The Baratron (0.001−10 Torr) pressure transducer was used for the low-pressure measurements. Collected isotherm points have been corrected for thermal transpiration effect. For Ar adsorption isotherms at 77 K, the saturation pressure of the supercooled liquid Ar has been used. There is experimental[16] and theoretical evidence[15] that Ar in narrow cylindrical pores at 77 K behaves as a liquid, rather than as a solid.

TABLE 1: Sample Codes of MCM-41 Catalyst Supports and V/MCM-41 Catalysts

siliceous MCM-41 sample code	vanadium MCM-41 sample code	surfactant
C8		$C_8H_{17}(CH_3)_3NOH$
C10		$C_{10}H_{21}(CH_3)_3NOH$
C12		$C_{12}H_{25}(CH_3)_3NOH$
C14	C14−$VOSO_4$[a]	$C_{14}H_{29}(CH_3)_3NOH$
	C14−V_2O_5[b]	$C_{14}H_{29}(CH_3)_3NOH$
C16	C16−$VOSO_4$[a]	$C_{16}H_{33}(CH_3)_3NOH$
	C16−V_2O_5[b]	$C_{16}H_{33}(CH_3)_3NOH$
reference[c]		$C_{16}H_{33}N(CH_3)_3Cl$

[a] Samples made by $VOSO_4 \cdot 3H_2O$. [b] Sample made by V_2O_5. [c] Reference sample has been prepared by S. C.Ó Domhnaill at Mainz University (see ref 14, sample C therein).

Theory

Nonlocal Density Functional Theory of Adsorption in M41S Materials. In the density functional theory approach, the grand potential (GP) of the fluid in a pore at a given temperature, T, and the chemical potential μ is a functional of the local fluid density $\rho(\mathbf{r})$:

$$\Omega[\rho(\mathbf{r})] = F[\rho(\mathbf{r})] - \int d\mathbf{r}\, \rho(\mathbf{r})(\mu - V_{ext}(\mathbf{r})) \qquad (1)$$

where $F[\rho(\mathbf{r})]$ is the intrinsic Helmholtz free energy functional and $V_{ext}(\mathbf{r})$ is the potential of pore walls.

In a perturbation fashion, the Helmholtz free energy functional is divided into the contribution from a reference system of hard spheres and the attractive contributions. In this work, a nonlocal density functional for the system of hard spheres due to Tarazona was used.[17] Attractive contributions were treated in a mean-field fashion:[12]

$$F[\rho(\mathbf{r})] = \int d\mathbf{r}\, \rho(\mathbf{r})[f_{id}(\rho(\mathbf{r})) + f_{ex}(\bar{\rho}(\mathbf{r}))] + \frac{1}{2}\int\int d\mathbf{r}\, d\mathbf{r}'\, \rho(\mathbf{r})\rho(\mathbf{r}')\Phi_{attr}(|\mathbf{r} - \mathbf{r}'|) \qquad (2)$$

where $f_{id}(\rho(\mathbf{r}))$ is an ideal gas contribution per molecule; $f_{ex}(\bar{\rho}(\mathbf{r}))$ is an excess free energy per molecule in the hard sphere fluid, which depends on the smoothed density $\bar{\rho}(\mathbf{r})$, defined as

$$\bar{\rho}(\mathbf{r}) = \int d\mathbf{r}'\, \rho(\mathbf{r}')\omega(|\mathbf{r} - \mathbf{r}'|, \bar{\rho}(\mathbf{r})) \qquad (3)$$

where $\omega(|\mathbf{r} - \mathbf{r}'|)$ is a weighting function.[17]

The attractive contributions were modeled with the LJ 12-6 potential, split according to the Weeks−Chandler−Andersen prescription in its minimum $r_m = 2^{1/6}\sigma$:[18]

$$\Phi_{attr}(r) = \begin{cases} -\epsilon_{ff}, & r < r_m \\ \Phi_{l,j}(r), & r_m < r < r_c \\ 0, & r > r_c \end{cases} \qquad (4)$$

where r_c is a cutoff distance.

TABLE 2: Parameters of the NLDFT Model for N_2 and Ar Adsorption on MCM-41

adsorbate	ϵ_{ff}/k_B, K	σ_{ff}, Å	d_{HS}, Å	r_{cut}, Å	$\rho_S\,\epsilon_{sf}/k_B$, K/Å^2	σ_{sf}, Å
N_2	94.45	3.575	3.575	$5\sigma_{ff}$	20.33	3.494
Ar	118.05	3.305	3.38	$5\sigma_{ff}$	26.2	3.0

[a] ρ_s is the surface number density.

Parameters of the NLDFT Model for N_2 and Ar. The parameters of the LJ potential (ϵ_{ff} and σ_{ff}) and the diameter of the hard spheres d have been chosen to describe the bulk liquid−gas coexistence for N_2 and Ar at low temperatures.[14,15] This implies that the theory predicts liquid−gas coexistence densities, saturation pressure, and the surface tension of the free liquid−gas interface.[15]

Solid−fluid interactions were modeled with the 12-6 LJ potential, integrated over the cylindrical surface and accounting for the curvature of the cylindrical pores.[19] For an infinitely wide pore, this potential reduces to the 10-4 potential. The parameters of the external potential (ρ_s, ϵ_{sf}, and σ_{sf}) have been chosen in order to fit the N_2 and Ar standard isotherms on nonporous siliceous materials in the multilayer adsorption region.[9,20] Parameters of the NLDFT model are summarized in Table 2.

Minimization of the grand potential functional (eq 1) has been performed by the method of indeterminate Lagrange multipliers (ILM).[13] A more detailed description of the NLDFT model is given in refs 14 and 15.

Calculation of Pore Size Distributions from the NLDFT Model. The theory predicts the adsorption and desorption isotherms in individual pores, as well as the relative pressure P/P_0, corresponding to the equilibrium thermodynamic transition. In cylindrical symmetry, the excess isotherm per unit of pore volume is calculated from the density profile as

$$N_V(P/P_0) = \frac{8}{D^2}\int_0^{D/2} r\,\mathrm{d}r\,(\rho(r) - \rho_b) \tag{5}$$

where ρ_b is an equilibrium bulk density and D is the internal pore diameter. The internal pore diameter has been defined as

$$D = D_{c-c} - \Delta \tag{6}$$

where D_{c-c} is the diameter measured between the centers of the first layer of solid atoms, and Δ is the effective diameter of solid atoms, treated as hard spheres. The effective diameter of solid atoms has been defined from the combining rule:

$$\Delta = 2\left(\sigma_{sf} - \frac{1}{2}\sigma_{ff}\right) \tag{7}$$

using σ_{sf} and σ_{ff} for N_2.

Having a set of equilibrium model isotherms in individual pores, the experimental isotherm can be described by the so-called generalized adsorption isotherm equation (GAI) as a superposition of the model isotherms and the pore size distribution:

$$N_{exp}(P/P_0) = \int_{D_{min}}^{D_{max}} \varphi(D) N_{DFT}(D,P/P_0)\,\mathrm{d}D \tag{8}$$

where $N_{exp}(P/P_0)$ is the experimental isotherm, $N_{DFT}(D,P/P_0)$ is the theoretical isotherm in model pore of size D, and $\varphi(D)$ is the pore size distribution.

In the case of adsorption in an open cylindrical capillary, the desorption branch of the experimental isotherm is most likely to be the thermodynamically stable one.[21,22] Therefore, PSDs have been calculated from the desorption branches of the experimental isotherms.

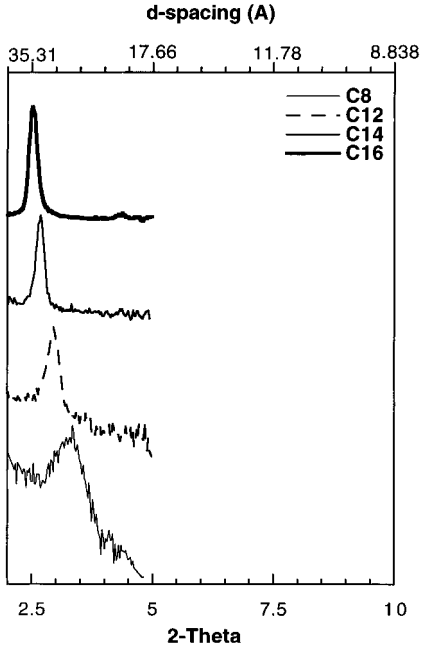

Figure 1. XRD patterns of pure siliceous MCM-41 samples.

Solution of the GAI have been obtained by transforming the integral eq 8 into a linear matrix equation:

$$\mathbf{N} = \mathbf{A}\mathbf{f} \tag{9}$$

where **A** is a kernel matrix whose columns are theoretical isotherms, **N** is the vector of an experimental isotherm, and **f** is the vector of the pore size distribution to be determined. Solutions have been calculated by using the original algorithm of nonnegative least squares (QNNLS), which involves the singular value decomposition (SVD) of the matrix **A**.[23] It will be shown below, that similarity between isotherms on MCM-41 in the region below the capillary condensation transition and the isotherm on nonporous substrate can be used to simplify solution of the GAI.

Results and Discussion

X-ray Diffraction. The uniform hexagonal pore structure of MCM-41 is reflected in a set of peaks in the low-angle XRD spectrum (2−10 of 2θ). From the XRD profiles of siliceous MCM-41 and vanadium substituted MCM-41, which are shown, respectively, in Figures 1 and 2, we observe only one intense peak in the low-angle range representing the spacing of the pores. Except for the siliceous sample C16, other peaks are not clearly seen. The hexagonal unit cell parameter a_0, a measure of spacing between the hexagonal layers, is calculated as the $d_{100}(2/\sqrt{3})$. This parameter is related to the average distance between pores in a two-dimensional framework, and for an ideal structure the parameter is equal to the internal pore diameter plus the thickness of pore walls. For pure siliceous samples, the values of a_0 vary in accord with the surfactant chain length (Table 3). The XRD signals become broader as the pore size decreases for siliceous MCM-41, indicating higher regularity of the samples with larger pores (C14-, C16-surfactants). By using the synthesis procedure indicated above, a slight decrease of the unit cell dimensions was observed with the addition of vanadium into the framework of C14−MCM-41 (samples C14−V_2O_5 and C14−$VOSO_4$) and C16−MCM-41 (sample C16−$VOSO_4$), despite the longer bond distance of

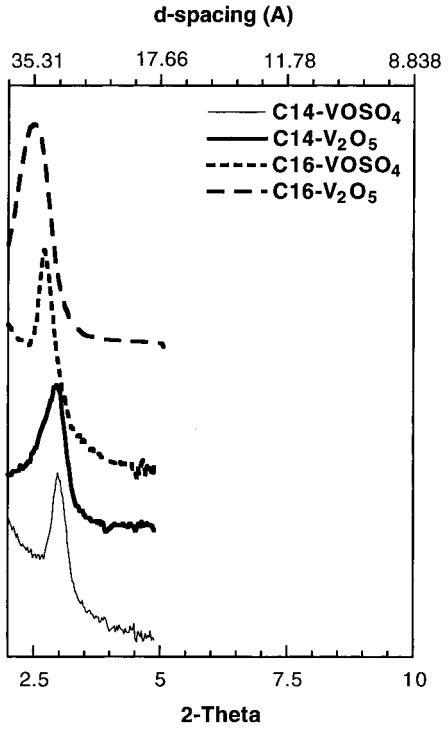

Figure 2. XRD patterns of vanadium-substituted MCM-41 samples.

V−O compared with that of Si−O. This might be caused by a bond angle contraction after the calcination. In contrast, a slight increase of the unit cell dimensions was observed for the sample C16−V_2O_5.

Reference MCM-41 Sample. In order to construct the comparative plots, it is useful to employ isotherms on a well-characterized MCM-41 sample as a reference. We used here isotherms on the sample described in ref 14 (sample C therein). The nitrogen and argon isotherms on the reference MCM-41 are presented in Figure 3. The isotherms are reduced to unit area, based on the BET surface area, determined from nitrogen isotherms, using the standard value of 0.162 nm^2 for the molecular cross sectional area of nitrogen. Comparative plots plotted versus the standard nitrogen and argon isotherms on nonporous hydroxilated silica were consistent with the previously published α_s plots[4] and confirmed the absence of micropores. The plots were linear down to $P/P_0 = 0.001$—the minimal relative pressure of the standard isotherms. The N_2 comparative plot for this sample was published in ref 14. More precise measurements (Figure 3) reveal a narrow but well-reproduced nitrogen hysteresis loop of type I. The argon isotherm exhibits a classical hysteresis loop of type I[9] with practically vertical adsorption and desorption branches. The difference in argon and nitrogen hysteresis loops is a consequence of the lower reduced temperature T/T_c of argon, where T_c is a bulk critical temperature (126.2 K for nitrogen and 150.9 K for argon).

The average pore size of the reference sample, calculated from the NLDFT model and taken as a maximum of the PSD curve, is ca. 45 Å. The X-ray diffraction data published previously[14] also indicated a uniform mesoporous structure with the hexagonal unit cell parameter $a_0 = 55.8$ Å which gives a pore wall thickness of 10.8 Å.

Siliceous MCM-41 Catalyst Supports. Nitrogen and argon isotherms on MCM-41 supports at 77 K are presented in Figures 4 and 5, respectively. In all cases, the steep portions of the argon isotherms are more sharp compare to nitrogen, and the argon isotherm on the C16 sample exhibits a hysteresis loop very similar in shape to that of the nitrogen isotherm on the reference sample. The amount adsorbed (in millimoles) after the steep increase of the isotherms is always higher because of the smaller size of the argon molecule.

Comparative Plots. Isotherms on the reference MCM-41 have been used to construct comparative plots (Figures 6 and 7). Isotherms on all samples are identical to the corresponding reference down to the lowest measurable pressure ($P/P_0 = 1 \times 10^{-5}$). All plots pass through the origin, indicating the absence of micropores. The upward deviations indicate the onset of capillary condensation. The pressures, P^*/P_0, of the beginning of capillary condensation vary in accordance with the surfactant chain length (see Table 3). The values P^*/P_0 are related to the smallest size of mesopores, in which the capillary condensation occurs. Inflection points on the steep portion of the isotherms correspond to the developed capillary condensation in mesopores. These pressures, P^{**}/P_0, are related to a characteristic pore size, which can be estimated theoretically, e.g., by means of the nonlocal density functional theory (NLDFT) (see ref 14 and Figure 9 therein).

The specific surface areas of mesopores have been determined from the comparative plots. Except probably for the sample C12, there is a fairly good agreement between surface areas determined from N_2 and Ar comparative plots (Table 3).

Calculation of Pore Size Distributions. From the comparative plots, it follows that adsorption per unit area on materials of various pore sizes is identical to the adsorption on the reference MCM-41 up to the relative pressures corresponding to the onset of the capillary condensation. This permits substitution of the NLDFT theoretical isotherms in the mono- and multilayer adsorption region, i.e., below the equilibrium transition point, with the corresponding isotherms on the reference MCM-41, while the transition pressure and further compacting of the fluid in the filled pore are described by the NLDFT. This approach describes correctly essential features of N_2 and Ar adsorption in the mesoporous molecular sieves of MCM-41 type and also simplifies the solution of the GAI. Thus, a whole experimental desorption isotherm can be fitted, and a nonnegative solution of the linear matrix equation can be obtained almost without employing a nonnegative least-squares algorithm. Of course, in this case the minimal pore diameter, D_{min}, is limited by the smallest pore size in which the capillary condensation mechanism is operative. In this model, the capillary critical pore size for N_2 adsorption at 77 K is ca. 18 Å.[14] It is worth noting that this pore size is traditionally regarded as a lower limit of mesopores.[9] This conclusion is based mainly on the analysis of N_2 isotherms at 77 K, and thus, NLDFT calculations confirm this traditional classification.

Comparison with the BJH and XRD Data. Pore size distributions are shown in Figures 8 and 9. The average pore sizes of samples C8−C16, taken as maximums of the PSD curves, vary in accord with the surfactant chain length and XRD data. We note a perfect agreement between the PSDs calculated from N_2 and from Ar isotherms by using NLDFT approach. For all pure siliceous MCM-41 samples, the average difference between the hexagonal unit cell parameter a_0 and NLDFT pore size is ca. 4−5.5 Å (Figure 10). This is slightly less than the commonly accepted thickness of the pore walls in MCM-41 of ca. 6−12 Å. The possible reason for this difference remains to be investigated. It should be noted that, in our case, interpretation of the XRD data rests on the assumption of an ideal hexagonal unit cell.

In contrast to the NLDFT results, the conventional BJH method[9] severely underestimates the calculated pore size by ca. 10 Å, resulting in a very large pore wall thickness of ca. 15−

TABLE 3: Structural Properties of Pure Siliceous and V/MCM-41 Samples

sample	gas	S_{BET}, m^2/g	S_{cmp}, m^2/g	P^*/P_0[a]	P^{**}/P_0[b]	NLDFT pore size,[c] Å	BJH pore size, Å	a_0, Å
C8	N_2		766	0.03	0.09	25	14.5	30.5
	Ar		787	0.02	0.1	24		
C10	N_2		1027	0.034	0.09	25	15.5	30.5
	Ar		1065	0.03	0.1	24		
C12	N_2	674	643	0.13	0.17	31	20	34.6
	Ar		750	0.17	0.18	31		
C14	N_2	926	904	0.13	0.24	34	22.5	38
	Ar		961	0.18	0.22	33		
C16	N_2	1090	1077	0.15	0.28	36	24	40.6
	Ar		1156	0.20	0.26	36		
C14-V_2O_5	N_2	1088	1096	0.11	0.21	33	21.2	34.5
	Ar		1104	0.08	0.21	33		
C16-V_2O_5	N_2	995	934	0.25	0.32	40	27.4	40.8
	Ar		1067	0.25	0.29	38		
C14−$VOSO_4$	N_2	1150	1027	0.15				34.6
	Ar		1155	0.20	0.29	38		
C16−$VOSO_4$	N_2	828	790	0.25				38.0
	Ar		806	0.27	0.33	42		

[a] P^*/P_0 is relative pressure of the beginning of the capillary condensation. [b] P^{**}/P_0 is mean pore size filling pressure according to NLDFT (using saturation pressure of the supercooled liquid for Ar). [c] Pore sizes have been calculated by using the cylindrical pore model.

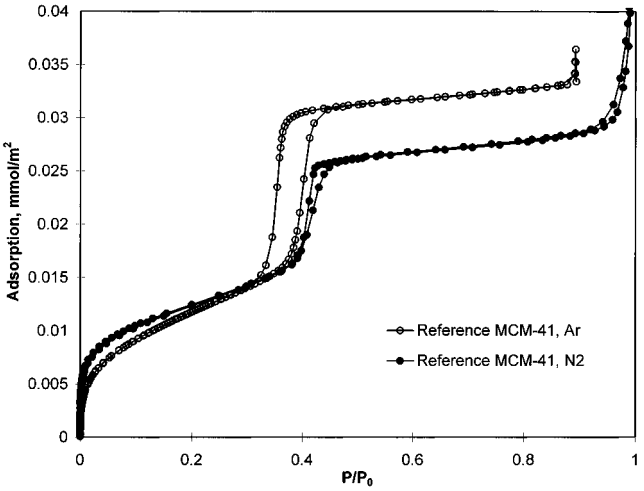

Figure 3. Nitrogen and argon isotherms on the reference MCM-41.

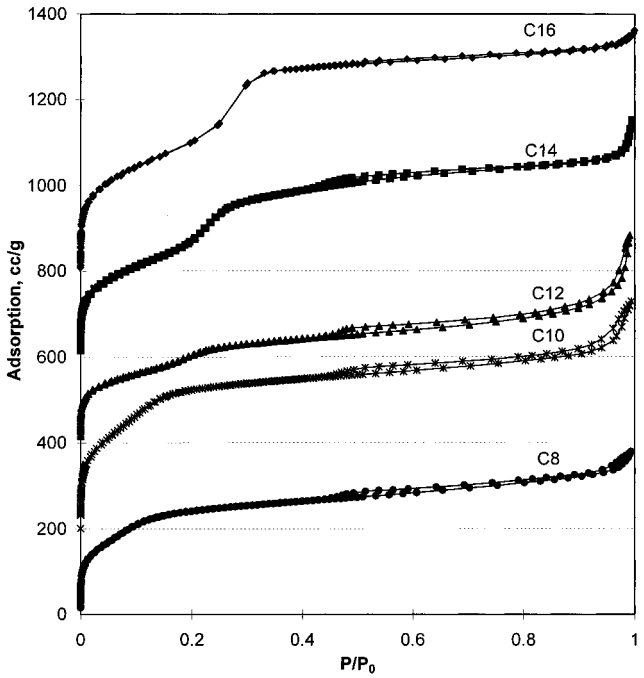

Figure 4. Nitrogen isotherms on siliceous MCM-41 samples at 77 K.

16 Å (Figure 10). It has been shown that, for ideal hexagonal samples with presumably uniform pores, NLDFT predicts pore wall thickness in MCM-41 of ca. 5−13 Å.[15] Our data also indicate that the thickness of pore walls in MCM-41 practically does not depend on the pore size.

V/MCM-41 Catalysts. *Samples Prepared with the Direct Addition of V_2O_5.* Nitrogen and argon isotherms on V/MCM-41 catalysts are presented in Figures 11 and 12. Comparative plots versus the isotherms on the reference MCM-41 (Figures 13 and 14) are linear down to the smallest relative pressure and pass through the origin, indicating the absence of any appreciable amount of micropores in all samples. For the samples prepared with the direct addition of V_2O_5 (C14−V_2O_5 and C16−V_2O_5), the first deviations from the linearity of the comparative plots (P^*/P_0) are observed at the point of the beginning of the steep increase in the isotherms, and the overall shapes of the isotherms is very similar to those on the corresponding pure siliceous samples (C14 and C16, respectively).

Pore size distributions (Figure 15) indicate that incorporation of vanadium into the framework of MCM-41 affects slightly the pore size in comparison with the pure siliceous sample made with the same surfactant. Again, an agreement between the N_2 and Ar pore size distributions obtained from NLDFT is very good. There is however some quantitative disagreement between the NLDFT pore size, calculated assuming the cylindrical pore model, and the hexagonal unit cell parameter a_0 obtained from XRD. This may be explained due to some nonuniformity of the pore structure, in which other pore regions, most likely slit-shaped pores, may be present along with the hexagonal pores. It has been shown[24,25] that there is an important quantitative difference in the adsorption isotherms in cylindrical and slitlike pores of the same material—the equilibrium transition in a slitlike pore of the same size as a cylindrical one occurs at substantially higher relative pressure. Also, the thermodynamic adsorption hysteresis in a slitlike pore is wider than that in the corresponding cylindrical pore. Therefore, the steep portion of the experimental isotherm may correspond to evaporation from both cylindrical and from slitlike pores of a smaller size. In this case the use of an ideal cylindrical pore model may lead to some overestimation of the calculated pore size. As was already noted, the repeating distance calculated from the XRD patterns assuming the hexagonal unit cell may also be inaccurate for the "nonideal" samples.

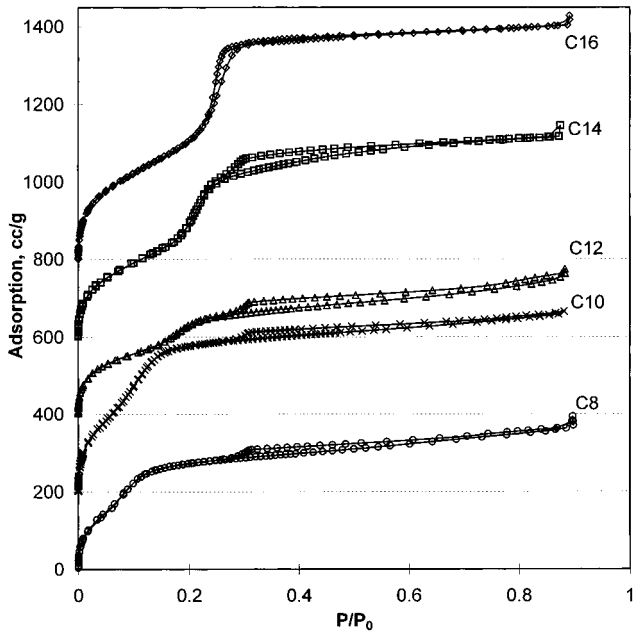

Figure 5. Argon isotherms on siliceous MCM-41 samples at 77 K.

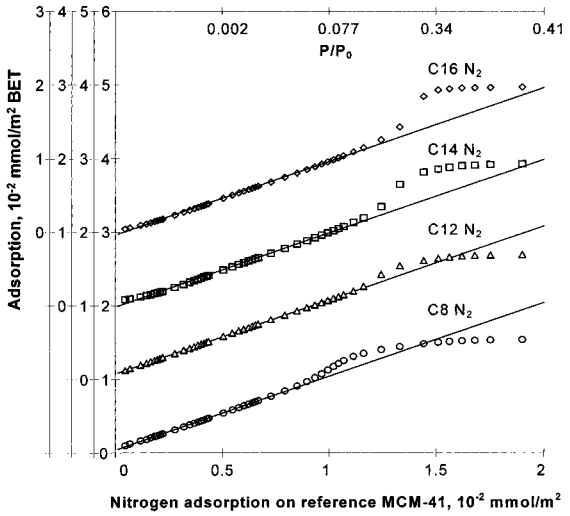

Figure 6. Comparative plots for the nitrogen adsorption at 77 K on siliceous MCM-41 supports versus adsorption on the reference MCM-41 sample: circles, C8; triangles, C12; squares, C14; rhombus, C16. The scale is shifted for convenience.

Samples Prepared with $VOSO_4 \cdot 3H_2O$. Isotherms on samples prepared with $VOSO_4 \cdot 3H_2O$ solution (samples C14−$VOSO_4$ and C16−$VOSO_4$) are of unusual shape (Figures 11 and 12). The isotherms form wide hysteresis loops. As expected, the hysteresis loop on the sample with bigger pore size (C16−$VOSO_4$) is more pronounced than for the smaller-size sample, C14−$VOSO_4$. Hysteresis loops for Ar are much wider than for N_2. Such hysteresis loops cannot be attributed to the desorption from a secondary macroporous structure (hysteresis loop of type III according to the IUPAC classification,[9] with a lower closure point for nitrogen hysteresis at P/P_0 of ca. 0.42). N_2 isotherms indicate that macropores are not present in these samples. The hysteresis loops on samples C14−$VOSO_4$ and C16−$VOSO_4$ are more close to the typical hysteresis loop on porous glasses.[25] In the C16−$VOSO_4$ sample, the greater part of N_2 desorbs at relative pressures P/P_0 from 0.51 to 0.42.

For both samples, the upward deviations of the N_2 comparative plots (Figure 13) occur well below the points of the beginning of the hysteresis loops. Accordingly, the N_2 isotherms exhibit a visible inclination at relative pressures P/P_0 below the

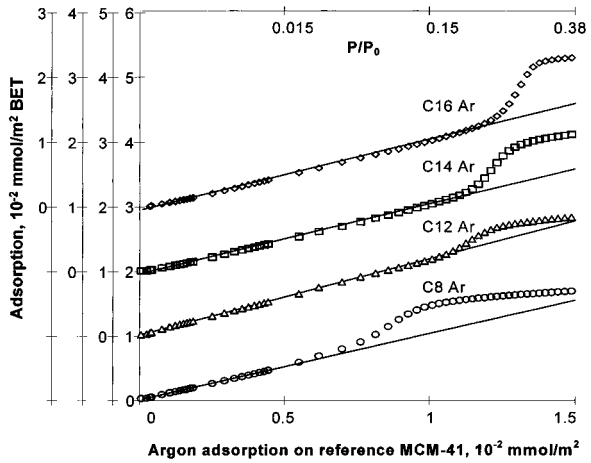

Figure 7. Comparative plots for the argon adsorption at 77 K on siliceous MCM-41 supports versus adsorption on the reference MCM-41 sample: circles, C8; triangles, C12; squares, C14; rhombus, C16. The scale is shifted for convenience.

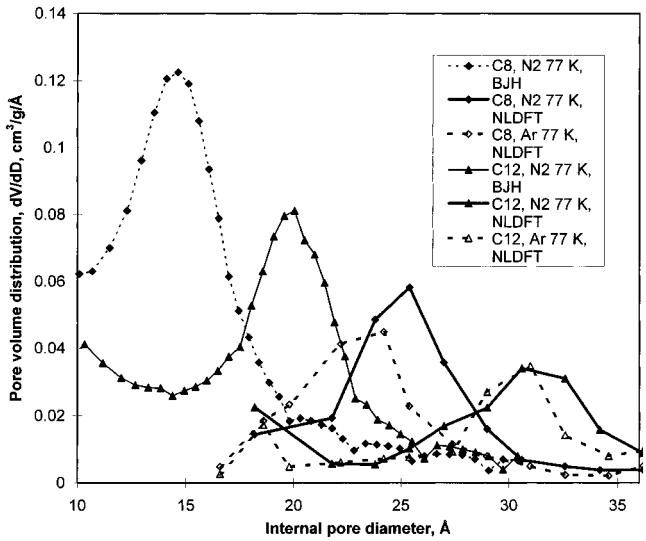

Figure 8. Pore size distributions in siliceous MCM-41 supports C8 and C12. Note that ordinates of the BJH plots are multiplied by 2 for convenience.

hysteresis. The comparative plots (Figure 13) indicate that the reversible capillary condensation begins well below the lower closure point of the hysteresis loop at $P^*/P_0 = 0.15$ for C14−$VOSO_4$ sample and at $P^*/P_0 = 0.25$ for C16−$VOSO_4$ sample (see Table 3).

The argon comparative plot for the sample C14−$VOSO_4$ (Figure 14) is linear up to the relative pressure 0.2 (Table 3), and the lower closure point of the hysteresis loop is ca. $P/P_0 = 0.27$. At the same time, the comparative plot for the C16−$VOSO_4$ sample is linear up to the beginning of the hysteresis loop.

The formal calculation of the pore size distributions from the *desorption* branches of the N_2 isotherms by using the NLDFT *cylindrical* pore model yields bimodal distributions (Figure 16) with the characteristic pore sizes of 34 and 47 Å in C14−$VOSO_4$ sample, and respectively, 39 and 49 Å in the C16−$VOSO_4$ sample. The first structures correspond to the characteristic pore sizes in pure siliceous materials C14 and C16. Pore size distributions obtained from Ar isotherms are unimodal (Figure 16).

These challenging data require further work. A possible explanation is that the structure is not homogeneous and that it contains an appreciable amount of slitlike pores and pores of

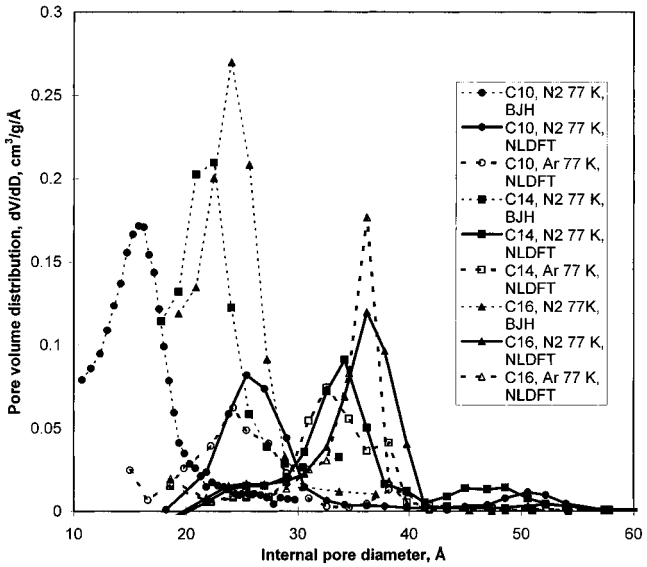

Figure 9. Pore size distributions in siliceous MCM-41 supports C10, C14, and C16. Note that ordinates of the BJH plots are multiplied by 2 for convenience.

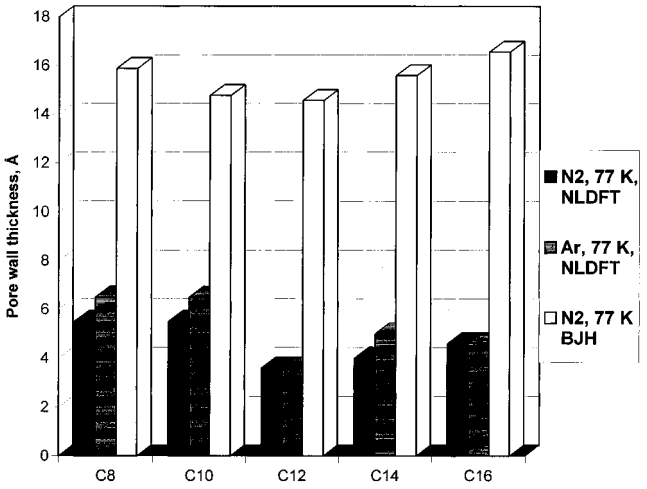

Figure 10. Pore wall thickness in siliceous MCM-41 samples as determined by subtracting from the hexagonal unit cell parameter a_0 the internal pore sizes calculated from adsorption data using NLDFT and BJH models.

other irregular shapes. Also, pore-blocking effects should not be completely disregarded, even though they are unlikely to happen in such materials. Thus, in this case application of the cylindrical pore model for calculating PSD is questionable. Our preliminary measurements of the scanning N_2 and Ar desorption isotherms on these samples show that the scanning curves exhibit unusual behavior.

It is however quite clear that the synthesis procedure with direct addition of V_2O_5 yields more uniform V-substituted samples. Thus, a comparative study of the V/MCM-41 catalysts with the same V content, but different pore structures (different source in synthesis) will provide an opportunity to assess pore structure on catalysis in mesoporous materials. This work will be reported later.

Conclusions

Siliceous MCM-41 catalyst supports and V/MCM-41 catalysts have been synthesized and characterized by N_2 and Ar adsorption. N_2 and Ar isotherms at 77 K have been measured starting from the relative pressure $P/P_0 = 1 \times 10^{-5}$. Comparative plots constructed versus N_2 and Ar isotherms on a well-characterized

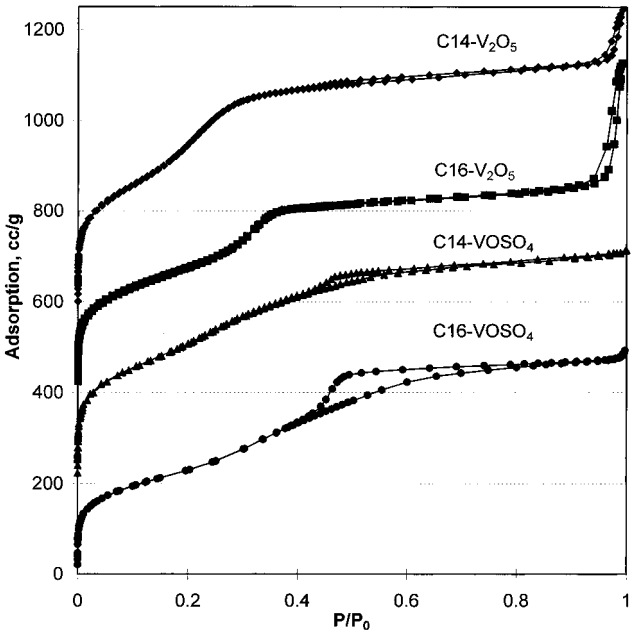

Figure 11. Nitrogen isotherms on V/MCM-41 catalysts at 77 K.

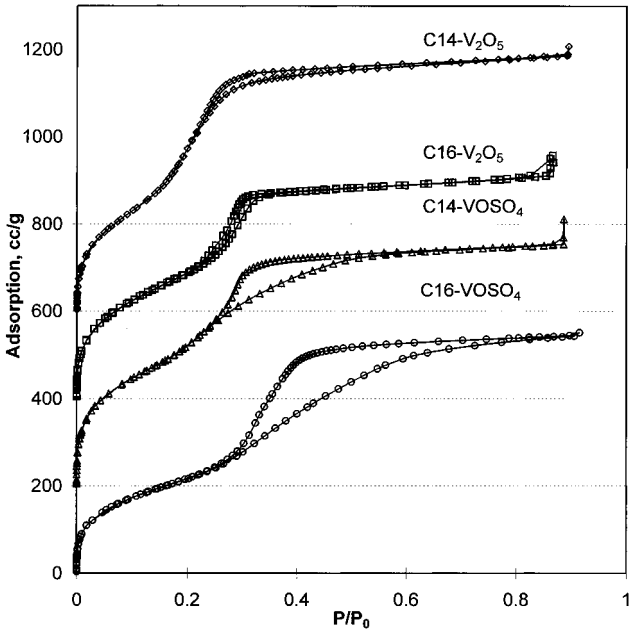

Figure 12. Argon isotherms on V/MCM-41 catalysts at 77 K.

reference MCM-41 sample showed that, for both gases, adsorption on all samples is identical to that on the reference sample at sufficiently low pressures. No appreciable amount of micropores have been found in any samples. The upward deviations of the comparative plots are observed in the region of capillary condensation. A capillary condensation mechanism of pore filling is operative on all samples, starting from the C8 sample with the smallest pore size of ca. 25 Å.

Pore size distributions have been calculated from the N_2 and Ar isotherms at 77 K based on the NLDFT model, assuming an ideal cylindrical pore structure. Ar in pores at 77 K was treated as a supercooled liquid rather than solid. Similarity of the experimental isotherms reduced per unit of pore area on the region preceding the capillary condensation was used to simplify calculations of PSDs, which have been obtained almost without using a nonnegative least squares fitting. Pore size distributions obtained from N_2 and Ar isotherms are in perfect agreement for all samples, except for V/MCM-41 catalysts

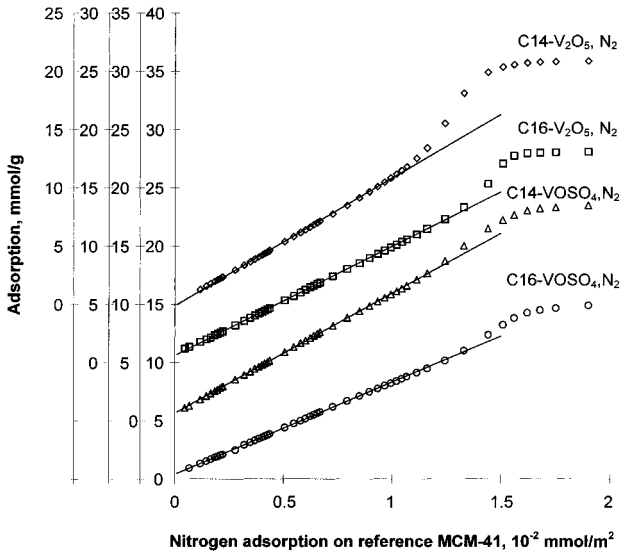

Figure 13. Comparative plots for the nitrogen adsorption at 77 K on V/MCM-41 catalysts versus adsorption on the reference MCM-41 sample: rhombus, C14−V_2O_5; squares, C16−V_2O_5; triangles, C14−$VOSO_4$; circles, C16−$VOSO_4$. The scale is shifted for convenience.

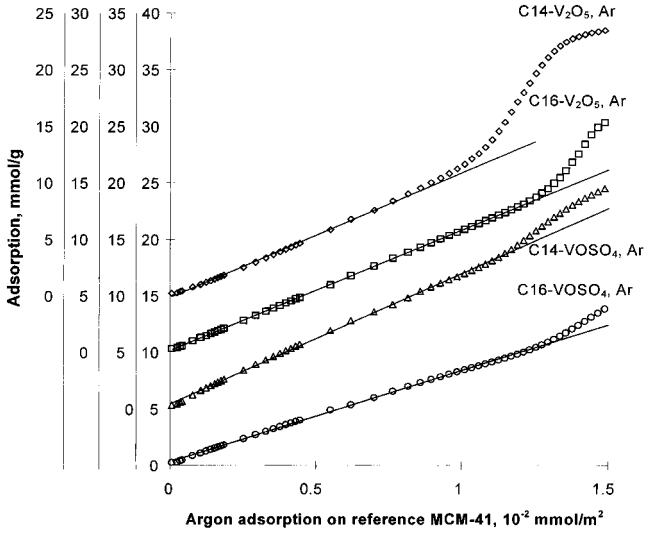

Figure 14. Comparative plots for the argon adsorption at 77 K on V/MCM-41 catalysts versus adsorption on the reference MCM-41 sample: rhombus, C14−V_2O_5; squares, C16−V_2O_5; triangles, C14−$VOSO_4$; circles, C16−$VOSO_4$. The scale is shifted for convenience.

prepared with the $VOSO_4 \cdot 3H_2O$ solution. This supports the consistency of the NLDFT method for calculating PSD. The calculated pore sizes vary in accordance with the surfactant chain length. A reasonable agreement between the XRD-spacing data, calculated on the basis of the hexagonal unit cell and the NLDFT pore sizes, has been found for pure siliceous MCM-41 samples. Comparison with the PSDs calculated from the conventional BJH method showed that the BJH method underestimate an average pore size by ca. 10 Å. It is worth noticing that other methods, for example, thermoporometry, also point toward bigger pore sizes in MCM-41 materials than those calculated from the Kelvin-based approach.[27]

Adsorption data indicate that the sythesis procedure with the direct addition of V_2O_5 yields V/MCM-41 samples with a more uniform structure than does the procedure with the use of $VOSO_4 \cdot 3H_2O$ solution. It should be noted that from the XRD patterns for "nonideal" samples it is hard to judge the uniformity of the pore structure, i.e., V/MCM-41 samples prepared from $VOSO_4 \cdot 3H_2O$ have more narrow diffraction peaks than those

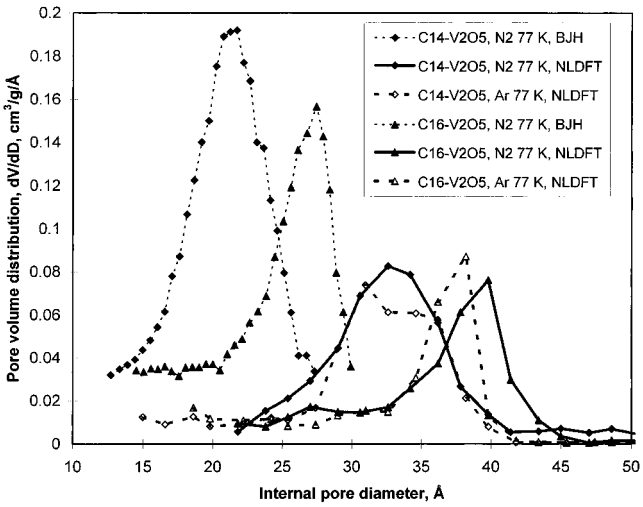

Figure 15. Pore size distributions in V/MCM-41 catalysts prepared from V_2O_5. Note that ordinates of the BJH plots are multiplied by 2 for convenience.

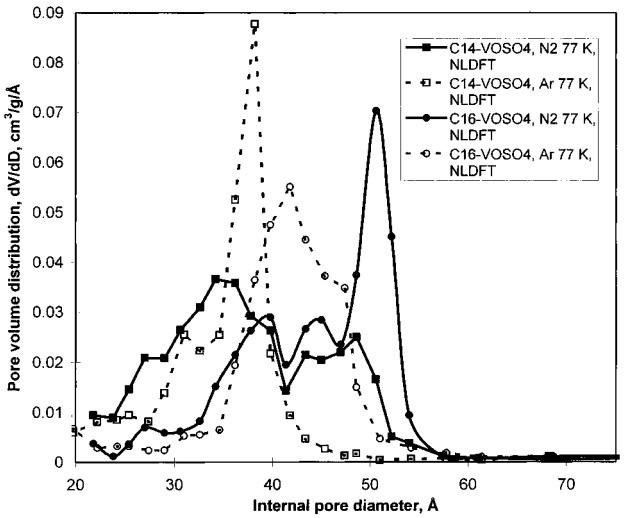

Figure 16. Pore size distributions in V/MCM-41 catalysts prepared from $VOSO_4 \cdot 3H_2O$.

prepared from V_2O_5, although analysis of the adsorption isotherms clearly indicate that the later are more ordered. Thus, adsorption is probably the most sensitive tool for evaluating quality and structural properties of the nanoporous materials of MCM-41 type.

Combination of the comparative method based on the reference isotherms on a well-characterized MCM-41 and the results of the NLDFT model are recommended for characterization of these materials.

Acknowledgment. We thank S. C. Ó Domhnaill, F. Schüth, and K. Unger for the MCM-41 sample used here as a reference. We thank Quantachrome Corporation, FL for the adsorption instrument. This work was supported, in part, by Grant DE-FG02-88ER13836 from DOE, Office of Basic Energy Sciences.

References and Notes

(1) Kresge, C. T.; Leonowicz, M. E.; Roth, W. J.; Vartuli, J. C.; Beck, J. S. *Nature* **1992**, *359*, 710.

(2) Beck, J. S.; Vartuli, J. C.; Roth, W. J.; Leonowicz, M. E.; Kresge, C. T.; Schmitt, K. D.; Chu, C. T.-W.; Olson, D. H.; Sheppard, E. W.; McCullen, S. B.; Higgins, J. B.; Schlenker, J. L. *J. Am. Chem. Soc.* **1992**, *114*, 10834.

(3) Kresge, C. T.; Leonowicz, M. E.; Roth, W. J.; Vartuli, J. C. U.S. Patent 5098684, 1992; U.S. Patent 5102643. Beck, J. S.; Vartuli, J. C.; Roth, W. J.; Leonowicz, M. E.; Kresge C. T.; et al. U.S. Patent 5108725, 1992.

(4) Branton, P. J.; Hall, P. G.; Sing, K. S. W.; Reichert, H.; Schüth, F.; Unger, K. K. *J. Chem.Soc.Faraday Trans.* **1994**, *90*, 2965.
(5) Reddy, K. M.; Moudrakovski, I.; Sayari, A. *J. Chem. Soc., Chem. Commun.* **1994**, 1059.
(6) Corma, A.; Navarro, M. T.; Pariente, J. P. *J. Chem. Soc., Chem. Commun.* **1994**, 147.
(7) Tanev, P. T.; Chibwe, M.; Pinnavala, T. J. *Nature* **1994**, *368*, 321.
(8) Ciesla, U.; Grün, M.; Isajeva, T.; Kurganov, A. A.; Neimark, A. V.; Ravikovitch, P. I.; Schacht, S.; Schüth, F.; Unger K. K. *Critical Appraisal of the Pore Structure of MCM-41*; Pinnavaia, T. J., Thorpe, M. F., Eds.; Plenum Press: New York, 1995; p 231−240.
(9) Gregg, S. J.; Sing, K. S. W. *Adsorption, Surface Area, and Porosity*; Academic Press: New York, 1982.
(10) Cracknell, R. F.; Gubbins, K. E.; Maddox, M.; Nicholson, D. *Acc. Chem. Res.* **1995**, *28*, 281.
(11) Seaton, N. A.; Walton, J. P. R. B.; Quirke, N. *Carbon* **1989**, *27*, 853.
(12) Lastoskie, C.; Gubbins, K. E.; Quirke, N. *J. Phys.Chem.* **1993**, *97*, 4786.
(13) Neimark, A. V. *Langmuir* **1995**, *11*, 4183.
(14) Ravikovitch, P. I; Ó Domhnaill, S. C.; Neimark, A. V.; Schüth, F.; Unger, K. K. *Langmuir* **1995**, *11*, 4765.
(15) Neimark, A. V.; Ravikovitch, P. I; Grün, M.; Schüth, F.; Unger K. K. in *Characterization of Porous Solids IV*; Elsevier: Amsterdam, 1996, in press.
(16) Llewellyn, P. L.;.Grillet, Y.; Rouquerol, J.; Martin, C.; Coulomb, J.-P. *Surf. Sci.* **1996**, *352*−*354*, 468.
(17) Tarazona, P. *Phys. Rev. A* **1985**, *31*, 2672; **1985**, *32*, 3148.
(18) Weeks, J. D.; Chandler, D.; Andersen, H. C. *J. Chem. Phys.* **1971**, *54*, 5237.
(19) Tjatjopoulos, G. J.; Feke, D. L.; Mann J. A., Jr. *J. Phys.Chem.* **1988**, *92*, 4006.
(20) Gobet, J.; Kováts, E.sz. *Ad. Sci. Tech.* **1984**, *1*, 285.
(21) Ball, P. C.; Evans. R. *Langmuir* **1989**, *5*, 714.
(22) Neimark, A. V.; Ravikovitch, P. I.; Ó Domhnaill, S. C.; Schüth, F.; Unger, K.K. In *Fundamentals of Adsorption*; LeVan, M. D., Ed.; Kluwer: Boston, 1996; p 667.
(23) Forsythe, G. E.; Malcolm, M. A.; Moler, C. B. *Computer methods for Mathematical Computaions*; Prentice-Hall: Englewood Cliffs, NJ, 1977.
(24) Evans, R.; Marini Bettolo Marconi, U.; Tarazona, P. *J. Chem. Soc., Faraday Trans. 2* **1986**, *82*, 1763.
(25) Ravikovitch, P. I.; Neimark, A. V.; Schacht, S.; Schüth, F.; Unger, K. K. In AIChE Topical Conference, *Recent Developments and Future Opportunities in Separation Technology*, Miami, FL, November 12−17, 1995; American Institute of Chemical Engineers: New York, 1995; Vol. 2, p 11.
(26) Everett, D. H. In *The Solid-Gas Interface*; Flood, E. A., Ed.; Marcel Dekker: New York, 1967; Vol. 2, p 1068.
(27) Kloetstra, K. R.; Zandbergen, H. W.; van Koten, M. A.; van Bekkum, H. *Catal. Lett.* **1995**, *33*, 145.